Earth and Planetary Science Letters 465 (2017) 145–154

Contents lists available at ScienceDirect

Earth and Planetary Science Letters

www.elsevier.com/locate/epsl

Origin of crystalline silicates from Comet 81P/Wild 2: Combined study on their oxygen isotopes and mineral chemistry

Céline Defouilloy [a,*], Daisuke Nakashima [b], David J. Joswiak [c], Donald E. Brownlee [c], Travis J. Tenner [a,1], Noriko T. Kita [a]

[a] WiscSIMS, Department of Geoscience, University of Wisconsin–Madison, Madison, WI 53706, USA
[b] Division of Earth and Planetary Materials Science, Tohoku University, Miyagi 980-8578, Japan
[c] Department of Astronomy, University of Washington, Seattle, WA 98195, USA

ARTICLE INFO

Article history:
Received 25 August 2016
Received in revised form 28 January 2017
Accepted 25 February 2017
Editor: B. Marty

Keywords:
oxygen isotope ratios
crystalline silicate
comet 81P/Wild 2
solar system formation
Stardust

ABSTRACT

In order to explore the link between comet 81P/Wild 2 and materials in primitive meteorites, seven particles 5 to 15 μm in diameter from comet 81P/Wild 2 have been analyzed for their oxygen isotope ratios using a secondary ion mass spectrometer. Most particles are single minerals consisting of olivine or pyroxene with Mg# higher than 85, which are relatively minor in 81P/Wild 2 particles (~1/3 of the ^{16}O-poor cluster). Four particles extracted from Track 149 are ^{16}O-poor and show $\Delta^{17}O$ ($=\delta^{17}O-0.52\times\delta^{18}O$) values from −2‰ to +1‰, similar to previous studies, while one enstatite (En_{99}) particle shows lower $\Delta^{17}O$ value of -7 ± 4‰ (2σ). This compositional range has not been reported among ^{16}O-poor particles in 81P/Wild 2, but is commonly observed among chondrules in carbonaceous chondrites and in particular in CR chondrites. The distribution in $\Delta^{17}O$ indicates that ^{16}O-poor 81P/Wild 2 particles are most similar to chondrules (and their fragments) in the CR chondrites and Tagish Lake-like WIS91600 chondrite chondrule silicate grains, which indicates that they likely come from a reservoir with similar dust/ice ratios as CR chondrites and WIS91600. However, differences in the Mg# distribution imply that the 81P/Wild 2 reservoir was comparatively more oxidized, with a higher dust enrichment. Two nearly pure enstatite grains from track 172 are significantly enriched in ^{16}O, with $\delta^{18}O$ values of -51.2 ± 1.5‰ (2σ) and -43.0 ± 1.3‰ (2σ), respectively, and $\Delta^{17}O$ values of -22.3 ± 1.9‰ (2σ) and -21.3 ± 2.3‰ (2σ), respectively. They are the first ^{16}O-rich pyroxenes found among 81P/Wild 2 particles, with similar $\Delta^{17}O$ values to those of ^{16}O-rich low-iron, manganese-enriched (LIME) olivine and CAI (calcium and aluminum-rich inclusions) – like particles from 81P/Wild 2. The major element and oxygen isotopic compositions of the pyroxenes are similar to those of enstatite in amoeboid olivine aggregates (AOAs) in primitive chondrites, in which ^{16}O-rich pyroxenes have previously been found, and thus suggest a condensation origin.

1. Introduction

In 2006, the Stardust spacecraft returned to Earth a precious cargo of comet particles collected during a close fly-by of the Jupiter Family Comet (JFC) 81P/Wild 2. Expectations were that the particles, coming from cold regions of the Solar System, would provide new insights on the characteristics of the outer solar system and would predominantly be composed of presolar interstellar grains (Greenberg and Li, 1999). However, close examination of the returned samples revealed an unexpected assemblages. If a few presolar grains (Messenger et al., 2009; Leitner et al., 2010) and organic matter (Sandford et al., 2006; Matrajt et al., 2008) were found, the majority of the collected particles resembled chondritic materials. Numerous high-temperature materials were collected, such as Ca, Al-rich inclusions (CAIs; e.g. Zolensky et al., 2006; Joswiak et al., 2012) and ferromagnesian chondrule fragments (Nakamura et al., 2008; Gainsforth et al., 2015; Bridges et al., 2012; Joswiak et al., 2012; Nakashima et al., 2012; Ogliore et al., 2012).

The oxygen isotope ratios of 81P/Wild 2 particles span a large range in delta notation (where $\delta^{17,18}O=[(R_{sample}/R_{VSMOW})-1]\times1000$; $R=^{17,18}O/^{16}O$; and VSMOW = Vienna Standard Mean Ocean Water). $\delta^{18}O$ and $\delta^{17}O$ values of >2 μm crystalline particles vary from −55‰ to +6‰, and $\Delta^{17}O$ ($=\delta^{17}O-0.52\times\delta^{18}O$) varies from −27‰ to +2.5‰ (McKeegan et al., 2006;

* Corresponding author.
E-mail address: defouilloy@wisc.edu (C. Defouilloy).
[1] Current address: Chemistry Division, Nuclear and Radiochemistry, Los Alamos National Laboratory, MSJ514 Los Alamos, NM 87545, USA.

http://dx.doi.org/10.1016/j.epsl.2017.02.045
0012-821X/

Nakamura et al., 2008; Nakamura-Messenger et al., 2011; Bridges et al., 2012; Ogliore et al., 2012, 2015; Nakashima et al., 2012; Joswiak et al., 2014; Gainsforth et al., 2015). Particles smaller than 2 μm show even larger variations, with $\Delta^{17}O$ ranging from −80‰ to +60‰ (Ogliore et al., 2015). All 81P/Wild 2 data plot on a slope ∼1 mixing line when comparing $\delta^{17}O$ vs. $\delta^{18}O$, similar to CCAM (Carbonaceous Chondrite Anhydrous Minerals; Clayton et al., 1977) or PCM (Primitive Chondrule Minerals; Ushikubo et al., 2012) lines. In a 3 oxygen isotope plot ($\delta^{17}O$ vs. $\delta^{18}O$), >2 μm particles form two clusters of data. The first one, representing ^{16}O-poor chondrule-like minerals, shows $\Delta^{17}O$ values of −5‰ to +2.5‰. The second cluster varies from $\Delta^{17}O = -24‰$ to −20‰ and is composed of CAI-like particles, LIME (low-iron, manganese-enriched) olivines and relict olivine grains in the chondrule-like objects (McKeegan et al., 2006; Nakamura et al., 2008; Nakashima et al., 2012).

The redox environment during the formation of crystalline silicate particles can be examined by the Mg# (mol% MgO/[MgO + FeO]) of olivine and pyroxene, which is related to the amount of iron distributed between metal and oxide (FeO) incorporated into the silicate grains (e.g., Tenner et al., 2015). In primitive chondrites, the Mg# of olivine and pyroxene in chondrules varies from 40 to 100 (Connolly and Huss, 2010; Kita et al., 2010; Rudraswami et al., 2011; Ushikubo et al., 2012; Schrader et al., 2013; Tenner et al., 2013, 2015). Based on their constituent olivine and/or pyroxene Mg#'s, chondrules are sorted into two groups: type I chondrules (FeO-poor, reduced), which have Mg#'s between 90 and 100, and type II chondrules (FeO-rich, oxidized) with Mg#'s < 90. The composition of 81P/Wild 2 silicate grains covers a similar range of Mg# as silicates found in various chondrite chondrules, though chondrules contain more grains with type I characteristics (Frank et al., 2014). Studies have shown distinctive Mg#–$\Delta^{17}O$ trends between different groups of chondrite chondrules (Connolly and Huss, 2010; Kita et al., 2010; Weisberg et al., 2011; Nakashima et al., 2012; Ushikubo et al., 2012; Schrader et al., 2013; Tenner et al., 2013, 2015). In ordinary and enstatite chondrites, $\Delta^{17}O$ values of chondrules are mostly zero or positive and are constant as a function of Mg#. In contrast, chondrules from carbonaceous chondrites show mostly negative $\Delta^{17}O$ values that show group specific correlations with Mg#. In CR chondrite chondrules, $\Delta^{17}O$ values of type I chondrules increase with decreasing Mg# from −6‰ to ∼0‰ (Tenner et al., 2015). This has been explained by the addition of water ice with positive $\Delta^{17}O$ values as an oxidant to anhydrous dust with a $\Delta^{17}O$ value ∼−6‰. Tenner et al. (2015) hypothesized that chondrules with the highest Mg#'s (≥98) and $\Delta^{17}O$ values of −6‰ to −4‰ are commonly observed among many different groups of carbonaceous chondrites, which would have formed in relatively anhydrous conditions in the protoplanetary disk. Similarly, ungrouped Acfer 094 and CO3.0 Yamato 81020 show bimodal distributions with $\Delta^{17}O \sim -5‰$ for particles with Mg# > 97 while particles with Mg# <97 have $\Delta^{17}O \sim -2‰$.

The combination of mineralogy, chemistry and O isotopes can help constrain the sources of crystalline silicates in the protoplanetary disk, and in particular the comparison of the Mg#–$\Delta^{17}O$ trend in 81P/Wild 2 particles with those of chondrules in various groups of chondrites. One possibility is that 81P/Wild 2 particles derived from silicates that migrated from the inner disk, either by radial diffusion (Ciesla, 2007), or by advection during the initial disk spreading (Yang and Ciesla, 2012). Alternatively, if these silicate particles crystallized beyond asteroid-forming regions, their data would reveal the variety of oxygen isotope reservoirs and/or redox states in the outer solar system. The total number of high precision oxygen isotope analyses on Stardust grains is still limited (<25) and spread over a large range of Mg# (99–60). Thus, more analyses are required to further explore links and differences between cometary and chondritic materials. Nakashima et al. (2012) show that there are some similarities between 81P/Wild 2 particles and CR chondrite chondrules. For instance, FeO-poor 81P/Wild 2 objects show $\Delta^{17}O$ of ∼−2‰ while FeO-rich 81P/Wild 2 objects show $\Delta^{17}O$ from −2‰ to +2‰. However, several CR chondrite chondrules have Mg#'s >97 with $\Delta^{17}O$ values of ∼−2‰ to −6‰, and particles with these characteristics have not been found in 81P/Wild 2. Moreover, CR chondrite chondrules are dominated by those with high Mg#'s (type I), which is much different from the broader distribution of Fo contents in olivine as reported by Frank et al. (2014). It is thus not clear if the ferromagnesian 81P/Wild 2 particles are truly related to CR chondrite chondrules, and/or other carbonaceous chondrites.

In addition to the lack of Mg# > 97 particles without ^{16}O-rich signatures (e.g. $\delta^{17,18}O \sim -50‰$), there are limited amounts of Stardust particle data in the Mg# 80–95 range, including no data from those having Mg#'s between 89 and 94 (Nakamura et al., 2008; Joswiak et al., 2012; Nakashima et al., 2012; Frank et al., 2014). We thus selected five new olivine and pyroxene particles with Mg# > 80. The $\Delta^{17}O$ values of these particles should test if the particles are related to refractory silicates (≤−20‰), or chondrule-like silicates from carbonaceous and ordinary chondrites (∼−6‰ to ∼+2‰).

To measure the O-isotope ratios, techniques for small spot analysis by secondary ion mass spectrometry (SIMS) are employed (Nakashima et al., 2011, 2012). In a previous study at the WiscSIMS laboratory, Nakashima et al. (2012) successfully analyzed 81P/Wild 2 particles as small as ∼4 μm by using FIB (Focused Ion Beam) marking and ^{16}O ion imaging. However, due to the limited 1 μm resolution of both stage motion and primary beam deflectors, the aiming was not highly accurate as small deviations between FIB marks and ion probe pits by as much as 0.5 μm were observed. For more accurate aiming, we made in-house modifications to the primary beam deflector and developed a new computer-programmable system called the "Nano-deflector", which enables deflecting the primary beam with 0.1 μm increments.

2. Analytical procedures

2.1. Sample preparation

Seven particles collected from comet 81P/Wild 2 were allocated by CAPTEM (Curation and Analysis Planning Team for Extraterrestrial Materials). To extract the particles from the Stardust spacecraft aerogel, each impact track was carefully cut out and divided into several slabs. Each slab contained a single particle. Five particles come from track 149 (Tona) from 5 distinct slabs (A, E, G, M, P) while two particles are from slabs B and C of track 172 (Wawa). The particles, ranging in size from 5 to 15 μm, are mounted in acrylic resin and ultramicrotomed for transmission electron microscope (TEM) analyses. They are selected for SIMS analyses because TEM analyses revealed that they contain coarse (>2 μm) olivine and low-Ca pyroxene with compositions of either high Mg# (≥95) or Mg# ∼ 85.

The particles remaining in the resin were extracted as a 100 μm wide acrylic cubes. Each cube was then pressed into a 1.4 mm diameter indium metal pool centered in an 8 mm aluminum disk, along with a San Carlos olivine standard (Nakashima et al., 2012). The accuracy of oxygen isotope analyses is highly dependent on the flatness of the sample surface, as even slight topography might cause a change in instrumental mass fractionation (Kita et al., 2009). To minimize the topography effects caused by sample holder edges, we used sample holders made of three 8 mm holes (Nakashima et al., 2011, 2012), allowing particles and standards to be positioned within 0.7 mm of the center of the mount.

2.2. Transmitted electron microscope analysis

Microtome sections of the samples were prepared for TEM at the University of Washington by cutting serial slices ~70 nm thick with a Leica Ultracut S ultramicrotome and placing them onto Au or Cu TEM grids containing 10 nm carbon films. They were placed into a double-tilt low-background Be sample holder which was inserted into a Tecnai 200 keV field emission TEM. The TEM is equipped with a CCD camera for bright- and dark-field imaging and secondary electron and high angle annular dark-field STEM detectors. Energy dispersive X-ray (EDX) spectra were acquired with an EDAX light element X-ray detector and quantified with EDAX Genesis software using standard thin-film k-factors obtained from natural minerals and the NIST SRM2063a thin-film standard. Spectral energy calibration was done using a Cu and Al thin-film prepared at the University of Washington. Maximum relative errors are estimated at 5% for major elements and 25–30% for most minor elements. High resolution lattice fringe images and electron diffraction patterns were obtained on some of the minerals to confirm atomic structures. Calibration of high resolution images was done using well-known mineral standards and an Al-thin film for diffraction camera lengths.

2.3. FIB-marking

Backscattered electron (BSE) images of the seven particles were obtained, prior to SIMS analyses, using a scanning electron microscope (SEM, Hitachi S3400) at the University of Wisconsin–Madison. Because the acrylic resin surrounding the sample is sensitive to alteration caused by electron beam damage, acquiring images can create depressions around the sample, and the infliction of surface topography might affect the instrumental mass fractionation during SIMS analyses (Kita et al., 2009). We minimized damage to the acrylic near the sample area by spending as little time as possible on the sample area at high magnification, while focusing BSE images on a region of the acrylic away from the comet particle. The positioning of targeted SIMS analysis regions for each grain was determined according to the BSE images. We used a Zeiss focused ion beam (FIB) field emission (FE)-SEM Auriga (UW-Madison) to mark the SIMS analysis positions by removing a 1 μm × 1 μm square of the carbon coating (SOM A). A focused Ga^+ beam with an accelerating voltage of 30 keV operated with a 5 pA beam current. A series of tests, previously performed, allowed us to determine that the right dosage to remove the 20-nm-thick carbon coating completely without sputtering the surface of the particle was 0.4 nC/μm^2 (equivalent to 90 s of sputtering with our settings). Previous test analyses showed no significant difference between standard analyses with or without FIB marks (Nakashima et al., 2012), so we did not apply FIB marks on any of the standard grains.

Prior to SIMS analysis, the topography of samples was checked to confirm that the SEM imaging did not alter the surface significantly. Profilometer images revealed that SEM imaging did not depress the acrylic surface by more than 1 μm around the comet particles.

2.4. Oxygen isotope analyses

Oxygen three-isotope ratios of the seven 81P/Wild 2 particles were acquired with the Cameca IMS 1280 ion microprobe at the WiscSIMS laboratory of the University of Wisconsin–Madison over two analytical sessions. The analytical conditions were similar to those in Nakashima et al. (2012). The primary Cs^+ beam was set at an intensity of 3 pA and beam size of ~1.5 μm in diameter.

Prior to each unknown sample analysis, secondary $^{16}O^-$ ion images were obtained in order to identify the FIB marks using 10 μm × 10 μm primary beam rastering (Nakashima et al., 2012). Due to the absence of carbon coating, the FIB marks appear as bright spots, allowing for easy centering of the mark to the image by first adjusting the stage, and then refining the centering with the NanoDeflector. Thanks to the recent addition of the NanoDeflector to the WiscSIMS IMS 1280, the adjustment of primary beam positioning (see SOM B for details) was greatly improved and the ion images were centered with a precision of 0.1 μm. We note that Nakashima et al. (2012) used a smaller primary beam (≤1 μm, 1 pA) for ion imaging to identify the FIB-mark, followed by a 3 pA beam condition (2 μm × 1 μm spot) for the isotope analysis. However, applying two different primary beam conditions between ion imaging and isotope analyses could potentially introduce a sub-μm level inaccuracy for the final sample aiming. The reason why the smaller beam was used for ion imaging is to obtain sharp images, to enable precise aiming (Nakashima et al., 2012). But even with 3 pA & 1.5 μm beam (this study), ion images were as sharp. Therefore, we used the same primary beam setting for ion imaging and for isotope analyses (3 pA, 1.5 μm). The centering of FIB mark by ion imaging took less than 5 min, and the removal of surface carbon coating was minimal. On two samples (T149/F7 and T172/F3), the FIB-marks were improperly adjusted due to a malfunction of the FE-SEM (Fig. SOM A). However, comparison between SEM images and SIMS ion images of misaligned FIB marks and the precision of the NanoDeflector aiming allowed us to locate SIMS analyses positions correctly (Fig. 1) without having to remove the coating and redo the FIB marks.

Secondary ions $^{16}O^-$, $^{17}O^-$, and $^{18}O^-$ were detected simultaneously on the multicollection system; $^{16}O^-$ by a Faraday cup (typical count rate ~1.6×10^6 cps, with a background noise of ~1×10^3 cps (2σ)) and $^{17}O^-$ and $^{18}O^-$ by electron multipliers (EM). The mass resolving power (MRP at 10% peak height) was set at ~6000 for ^{17}O and ~2200 for ^{16}O and ^{18}O. The contribution of tailing $^{16}O^1H^-$ ions on the $^{17}O^-$ signal was negligible (<0.1‰). Each analysis last 20 min, giving a typical internal precision of 1.2‰, 2.5‰ and 2.6‰ (2σ) for $\delta^{18}O$, $\delta^{17}O$, $\Delta^{17}O$, respectively.

One to six analyses were performed on each particle, bracketed by eight analyses performed on San Carlos olivine (Fo_{89}) grains mounted in the same disks, within 500 μm of the sample particle. The external reproducibility is calculated as twice the standard deviation (2σ) on the eight standard analyses bracketing the sample analyses, which represent spot-to-spot reproducibility and is assigned as uncertainty of individual analyses (Kita et al., 2009; Nakashima et al., 2012). They are generally very similar to the internal error of individual analyses, which is determined by FC detector background drift and counting statistics of minor isotopes using EM detectors, as well as a small drift of mass dependent fractionation with increasing analysis depth (Kita et al., 2009, 2010). The analytical uncertainty assigned to single spot analyses is calculated as the mean of the 2σ calculated for each set of the standard measurement brackets over the whole session. For samples with multiple measurements, we obtained the mean values. The uncertainty of the mean values is assigned as the propagation of (1) the maxima of the 2SD of sample data versus the analytical uncertainty of a single analysis, of which this value is divided by the square root of the number of analyses; (2) the 2SE (standard error of the mean) of the instrumental bias calculated from bracket standard analyses, and (3) uncertainties of instrumental mass-dependent fractionation across a 1 mm diameter of the 8 mm sample disk (0.5‰ in $\delta^{18}O$; Nakashima et al., 2012). The same error estimates of average values have been applied to SIMS chondrule analyses in previous studies (Ushikubo et al., 2012; Tenner et al., 2013, 2015). If only one analysis was made for a particle, we propagated uncertainties from (2) and (3) to the final value. The global external reproducibility of the running standards over the whole session was 1.4‰, 2.2‰, and 2.2‰ (2σ) for $\delta^{18}O$,

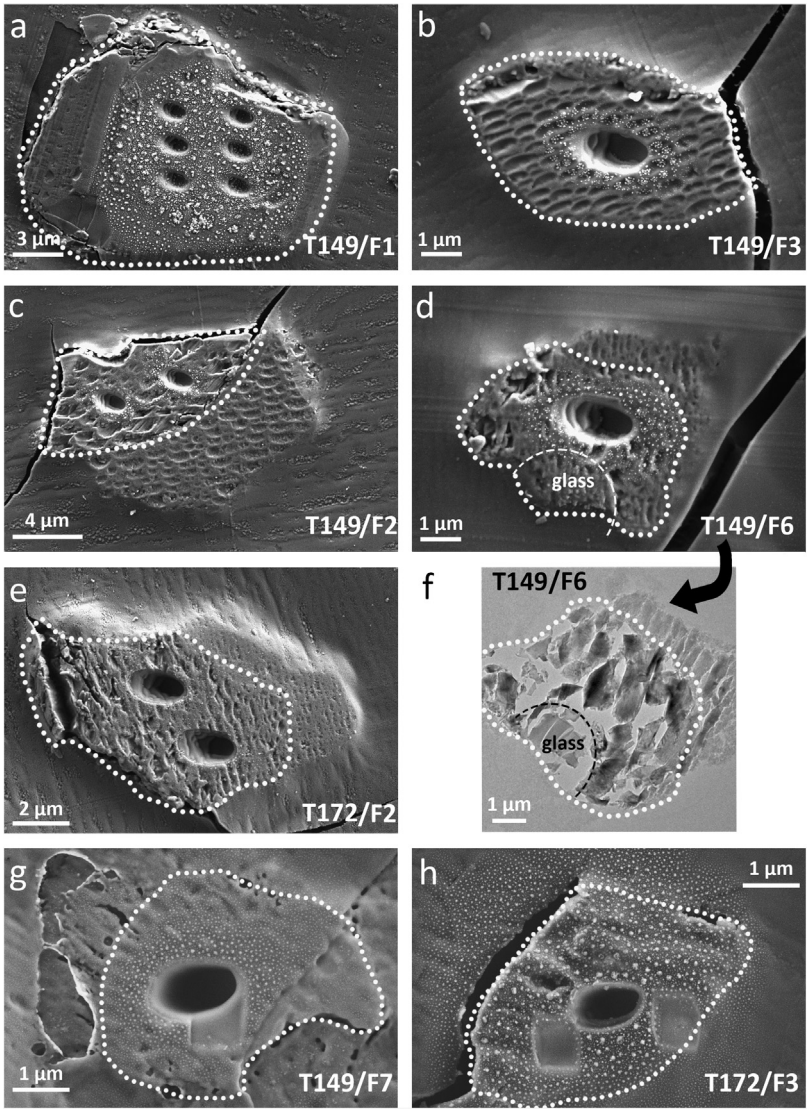

Fig. 1. Comet 81P/Wild 2 particles analyzed by SIMS in this study. (a–e, g–h) BSE images of the seven 81P/Wild 2 particles, after SIMS analyses. (a) T149/F1, (b) T149/F3, (c) T149/F2, (d) T149/F6, (e) T172/F2, (g) T149/F7, (h) T172/F3. SIMS pits are clearly visible, in lieu of the FIB-marks. (g) and (h) show the misaligned FIB-marks, still visible at the surface of the grains. (f) Bright field image of particle T149/F6, showing the position of the glass phase.

$\delta^{17}O$, $\Delta^{17}O$, respectively. Instrumental biases of olivine and pyroxene were calibrated using multiple standards (Fo_{60}, Fo_{89}, and En_{85} and En_{97}) with known oxygen isotope ratios that cover the range of compositions of the unknowns. Two geological glass standards (75.6% and 58.6% SiO_2) were also analyzed, to be used to correct for instrumental bias of unknown analyses in case it inadvertently overlapped with adjacent silica-rich glass (76.0% SiO_2). These data are reported in Table SOM C.

3. Results

3.1. Petrography and mineral chemistry

Track 149 is a ~4 mm-long bulbous track (Burchell et al., 2008) which is composed of a broad cavity, a long narrow root containing the terminal particle (T149/F1) and two short side roots containing fragments T149/F2 and T149/F3. Fragments T149/F6 and T149/F7 were located in the cavity near the base of the bulb. Track 172 is a ~0.9 mm-long bulbous track with a distinct narrow root containing the terminal particle. Fragments 2 (T172/F2) and 3 (T172/F3) were present at the termini of shorter side roots emanating from the bottom of the bulb and from the side of the main root, respectively. Major element compositions of microtome sections of the T149 and T172 particles are reported in Table 1. T149/F1 is a 10 × 13 µm olivine grain with a Mg# = 84.6, very similar to particle T149/F3 which is a 5 × 8 µm olivine grain with a Mg# of 86.0. Neither grains have a measurable amount of Al_2O_3. T149/F2 is a 7 × 12 µm pyroxene crystal with a Mg# = 99.5 ($En_{98.3}Wo_{1.2}$). T149/F6 is a 4 × 6 µm pyroxene grain accompanied by a small 1 × 2 µm glass phase. The Mg# of the pyroxene grain is of 94.7 ($En_{92.1}Wo_{2.7}$). T149/F2 contains slightly more Al_2O_3 than T149/F6 (1.61 wt% vs. 1.11 wt% respectively), and contains significantly less Cr_2O_3 (0.50 wt% vs. 1.24 wt%), FeO (0.35 wt% vs. 3.29 wt%) and MnO (0.08 wt% vs. 1.76 wt%) and moderately less CaO (0.63 wt% vs. 1.33 wt%). T149/F7 is a 5 × 7 µm fragment composed entirely of glass with an approximate enstatite composition (Mg# = 96.5). Finally, particles T172/F2 and T172/F3 are Mg# = 99.0 pyroxene grains ($En_{98.9}Wo_{0.1}$ and $En_{99}Wo_{0.3}$, respectively) with sizes of 5 × 9 µm and 4 × 5 µm, respectively. However, T172/F2 is distinctively more depleted in minor oxides (T172/F2: CaO = 0.04 wt%; T172/F3: Al_2O_3 = 0.52 wt%, CaO = 0.15 wt%).

Table 1
Major element compositions of the seven Wild 2 particles from track 149 and track 172 (normalized oxide wt%).

Track	Slab	Sample	Size (μm)	SiO_2	Al_2O_3	Cr_2O_3	FeO	MnO	MgO	CaO	Fo	Fs	En	Wo	Mg#
T149	A	T149/F1	18 × 23	39.73	b.d.	0.30	14.53	0.43	44.77	0.25	84.6	–	–	–	84.6
T149	E	T149/F2	7 × 12	60.24	1.61	0.50	0.35	0.08	36.60	0.63	–	0.5	98.3	1.2	99.5
T149	G	T149/F3	5 × 8	41.24	b.d.	0.42	13.02	0.49	44.68	0.16	86.0	–	–	–	86.0
T149	M	T149/F6	4 × 6	58.50	1.11	1.24	3.29	1.76	32.76	1.33	–	5.2	92.1	2.7	94.7
T149	P	T149/F7	5 × 7	63.39	b.d.	0.29	1.25	1.01	34.06	0.00	–	–	–	–	98.0
T172	B	T172/F2	5 × 9	58.49	b.d.	0.19	0.73	0.15	40.40	0.04	–	1.0	98.9	0.1	99.0
T172	C	T172/F3	4 × 5	57.86	0.52	0.29	0.57	0.20	40.41	0.15	–	0.7	99.0	0.3	99.3

b.d. = below detection.

Table 2
Oxygen isotope ratios of the seven Wild 2 particles.

Track	Slab	Sample	Analyse #	$\delta^{18}O$	2σ	$\delta^{17}O$	2σ	$\Delta^{17}O$	2σ
T149	A	T149/F1	1	3.6	1.3	−0.1	2.2	−1.9	2.5
			2	4.9	1.3	2.7	2.2	0.2	2.5
			3	3.6	1.3	1.3	2.2	−0.5	2.5
			4	4.8	1.3	1.1	2.2	−1.4	2.5
			5	4.5	1.3	−0.4	2.2	−2.8	2.5
			6	4.3	1.3	−1.5	2.2	−3.7	2.5
			average	**4.3**	**0.9**	**0.5**	**1.5**	**−1.7**	**1.5**
T149	E	T149/F2	1	−7.8	1.1	−13.0	2.0	−8.9	1.8
			2	−8.3	1.1	−9.1	2.0	−4.8	1.8
			average	**−8.1**	**1.0**	**−11.0**	**3.9**	**−6.8**	**4.2**
T149	G	T149/F3	1	6.6	1.5	4.0	2.4	0.6	2.4
T149	M	T149/F6	1	−2.1	1.5	−1.4	2.4	−0.3	2.4
T149	P	T149/F7	1	0.7	1.5	0.8	2.7	0.5	2.5
T172	B	T172/F2	1	−52.5	1.7	−50.5	2.5	−23.2	2.7
T172			2	−51.2	1.7	−48.1	2.5	−21.5	2.7
T172			**average**	**−51.9**	**1.5**	**−49.3**	**2.5**	**−22.3**	**2.1**
T172	C	T172/F3	1	−43.0	1.3	−43.6	2.4	−21.3	2.3

See text for error assignments.

3.2. Oxygen isotopes

A total of 155 analyses were collected over two sessions for a total of 14 analyses on Stardust grains. After the SIMS sessions, we inspected all analysis pits (on Stardust particles and San Carlos olivine standards) by SEM for irregularities and possible overlaps. SIMS aiming was highly accurate, with each pit covering its original FIB mark. No analysis points were rejected. In particular, a close inspection of particle T149/F6 containing glass, which was the most critical aiming-wise, revealed no overlap of pits with the glass phase or the aerogel. For all particles, the SIMS pits were located within <0.2 μm of their FIB-marks (Fig. 1), or at their intended locations within particles T149/F7 and T172/F3.

Oxygen isotope ratios of the seven particles are given in Table 2 and plotted in Fig. 2, reported as $\delta^{17,18}O = [(R_{sample}/R_{VSMOW}) - 1] \times 1000$; $R = {}^{17,18}O/{}^{16}O$ (VSMOW = Vienna Standard Mean Ocean Water). Oxygen isotope ratios vary from −52.5‰ to 6.6‰ in $\delta^{18}O$ and are distributed along a slope 1 line, as previous 81P/Wild 2 studies have shown (McKeegan et al., 2006; Nakamura et al., 2008; Nakamura-Messenger et al., 2011; Bridges et al., 2012; Ogliore et al., 2012, 2015; Nakashima et al., 2012; Joswiak et al., 2014; Gainsforth et al., 2015). We use the Primitive Chondrule Minerals (PCM) line for reference (Ushikubo et al., 2012), though our analytical precision does not resolve data from the CCAM (Carbonaceous Chondrite Anhydrous Mineral; Clayton et al., 1977) or Young and Russell (1998) lines. Three particles, T149/F1, T149/F2, and T172/F2, have data from multiple SIMS measurements. For T149/F1 and T172/F2, the data are indistinguishable within per-analysis uncertainties in $\delta^{18}O$ and $\delta^{17}O$. T149/F2 has two data points that differ by significantly more than the per-analysis uncertainties in $\delta^{17}O$ and $\Delta^{17}O$, and the uncertainties of the average reflect this.

As shown in Fig. 2, the particles extracted from track 149 all have ^{16}O-poor compositions on a three-isotope plot, with $\delta^{18}O$ varying from -8.1 ± 1.2‰ (T149/F2) to $+6.6 \pm 1.5$‰ (T149/F3), while $\Delta^{17}O$ varies from -6.9 ± 4.2‰ (T149/F2) to $+0.6 \pm 2.4$‰ (T149/F3). In contrast, the pyroxene grains from track 172 show significant enrichment in ^{16}O, with T172/F2 showing a $\delta^{18}O$ of -51.2 ± 1.5‰ and a $\Delta^{17}O$ of -22.3 ± 1.8‰ while T172/F3 dis-

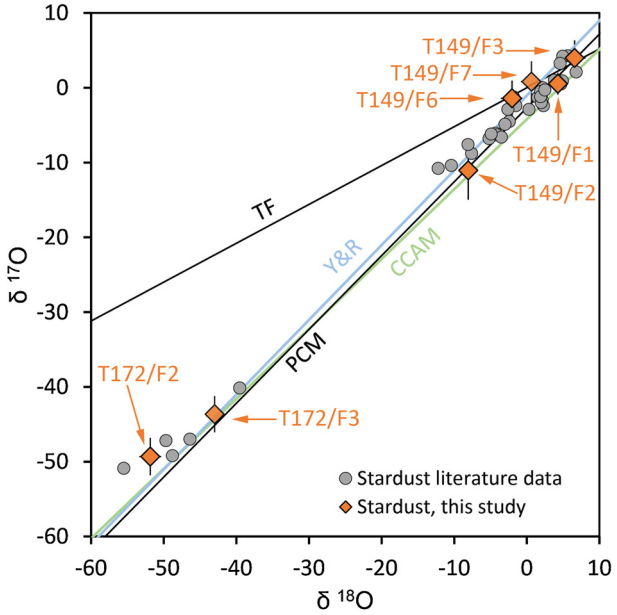

Fig. 2. Oxygen three-isotope ratios of the seven 81P/Wild 2 particles. TF, Y&R, CCAM and PCM represent the terrestrial fractionation line, the Young & Russell line, the carbonaceous chondrite anhydrous mineral line and the primitive chondrule line, respectively. Literature data from McKeegan et al. (2006), Nakamura et al. (2008), Nakamura-Messenger et al. (2011), Bridges et al. (2012), Ogliore et al. (2012), Nakashima et al. (2012).

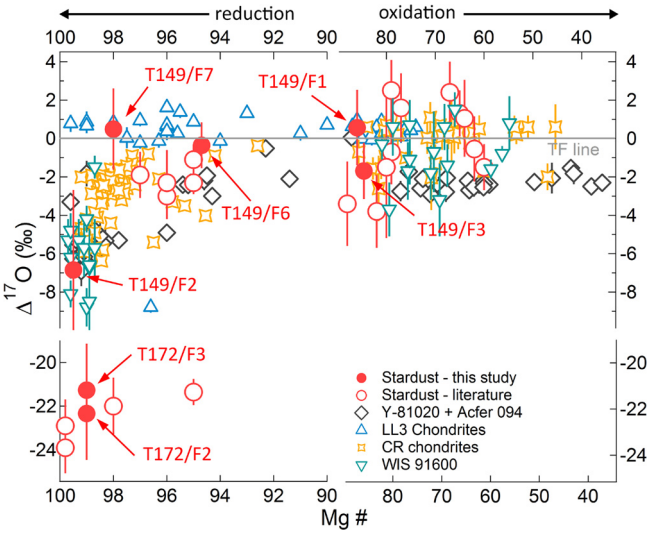

Fig. 3. Relationship between Mg# and $\Delta^{17}O$ in ferromagnesian 81P/Wild 2 particles and comparison to those in chondrules in primitive chondrites. Stardust literature data from McKeegan et al. (2006), Nakamura et al. (2008), Nakashima et al. (2012), and Ogliore et al. (2015). Yamato 81020 (CO3) data from Tenner et al. (2013), Acfer 094 (ungrouped C) data from Ushikubo et al. (2012), LL3 chondrite data from Kita et al. (2010), CR chondrite data from Connolly and Huss (2010), Schrader et al. (2013), and Tenner et al. (2015).

plays a $\delta^{18}O$ of -43.0 ± 1.3‰ and a $\Delta^{17}O$ of -21.3 ± 2.3‰. This enrichment is of the same order as other ^{16}O-rich particles found in 81P/Wild 2 particles (McKeegan et al., 2006; Nakamura et al., 2008; Nakashima et al., 2012).

4. Discussion

As the particles analyzed from track 149 have ^{16}O-poor signatures, while the two particles from track 172 have ^{16}O-rich characteristics, we discuss particles from tracks 149 and 172 separately below, due to their significant differences in oxygen isotope ratios.

4.1. Relationship between Mg# and $\Delta^{17}O$

Comet 81P/Wild 2 data from ^{16}O-poor ferromagnesian silicates show a correlation between $\Delta^{17}O$ and Mg#, with $\Delta^{17}O$ increasing as a function of decreasing Mg#, over a rather large range of $\Delta^{17}O$ (~−8‰ to ~+3‰; Fig. 3). Among chondrules in primitive chondrites, three main trends are observed: (1) in ordinary chondrites, $\Delta^{17}O$ remains nearly constant for most chondrules over the whole Mg# range, with an average of 0.5 ± 0.9‰ (2σ) except for rare ^{16}O-rich examples (Kita et al., 2010). (2) Ushikubo et al. (2012) showed that chondrules from the ungrouped type 3.0 carbonaceous chondrite Acfer 094 display two distinguishable oxygen isotope sub-groups, likely coming from two distinct oxygen isotope reservoirs: one chondrule sub-group is relatively ^{16}O-rich with a $\Delta^{17}O = -5.4 \pm 1.2$‰ ($2\sigma$) and Mg#'s > 96, and the other group is relatively ^{16}O-poor, with $\Delta^{17}O = -2.2 \pm 0.7$‰ ($2\sigma$) and Mg#'s of ~99–42. Similarly, Tenner et al. (2013) reported two distinct oxygen isotope groups among chondrules from the CO3.0 chondrite Yamato 81020: A "−5.5‰" chondrule group, showing $\Delta^{17}O$ varying from −4.8‰ to −6.5‰ for Mg#'s > 97 and a "−2.5‰" group displaying $\Delta^{17}O$ values of −2.1‰ to −3.0‰ for Mg#'s of ~96–36. (3) Among CR chondrites, Tenner et al. (2015) reported monotonic increases in $\Delta^{17}O$ with decreasing Mg# in type I chondrules (Mg# = 99 to 94), from $\Delta^{17}O$ values of −5.9‰ to −1‰, while type II chondrules show variable $\Delta^{17}O$ of −2‰ to +1‰ (Connolly and Huss, 2010; Schrader et al., 2013). For carbonaceous chondrites, the $\Delta^{17}O$ remains nearly constant for moderate Mg# chondrules (<96, type II), with an average value of 0.0 ± 2.0‰ (2σ) among those from CR chondrites (Connolly and Huss, 2010; Schrader et al., 2013; Tenner et al., 2015), and -2.2 ± 1.3‰ (2σ) among those from CO chondrite Yamato 81020 (Tenner et al., 2013) and the ungrouped Acfer 094 (Ushikubo et al., 2012). The $\Delta^{17}O$ values of high Mg# (Mg# ~96–99) chondrules are much lower than the above, with an average of −5‰. Tenner et al. (2015) hypothesized that the general trend of increasing chondrule $\Delta^{17}O$ with decreasing Mg# in most carbonaceous chondrite groups was caused by mixing between reduced anhydrous dusts ($\Delta^{17}O$: −6‰) and ^{16}O-poor H_2O ice (>0‰) in the chondrule-forming region of the protoplanetary disk, along with variable dust to gas ratios.

In the case of 81P/Wild 2 particles, all but one FeO-poor particle (Mg# > 97) show $\Delta^{17}O$ values of ~−2‰ and FeO-rich particles (Mg# < 97) vary between −4‰ and +2‰ (Fig. 3). We ran a series of statistical tests to determine which chondrite group had the most similar $\Delta^{17}O$ and Mg# distribution as 81P/Wild 2. The Kolmogorov–Smirnov test is a statistical test that compares the distributions of two sets of data (or one or two variables each). The p-value parameter translates how close the distributions are: a positive p-value means the distributions are similar, while a p-value ≈ 0 means that the distributions are distinct. The Kolmogorov–Smirnov test for one variable shows that the distribution of 81P/Wild 2 grains $\Delta^{17}O$ (mean = −1.8‰, σ = 2.1‰) is very close to the distribution of $\Delta^{17}O$ measured in CR chondrites chondrules (mean = −2.3‰, σ = 1.8‰) giving a p-value = 0.24, while it is clearly different from the $\Delta^{17}O$ distribution measured in OC chondrules (mean = −0.3‰, σ = 1.6‰) as well as chondrules from both Acfer 094 and Yamato 81020 (mean = −4.0‰, σ = 1.7‰) with a p-value ≈ 0 in both cases. The agreement among the range and variations between CR chondrites chondrule and 81P/Wild 2 grains suggests common precursor characteristics, including the mixing ratios between ^{16}O-poor water ice and ^{16}O-rich dust (Tenner et al., 2015). Tagish Lake-like chondrite WIS91600 (Yamanobe et al., 2016) shows a rather close distribution as well (mean = −3.1, SD = 3.1, p-value = 0.03), which indicates a similar precursor origin.

In addition to Mg# and O-isotope relationships, there are other indicators that 81P/Wild 2 particles and some chondritic materials originated from a common region of the protoplanetary disk. For instance, based on ^{26}Mg and ^{54}Cr isotopes, Van Kooten et al. (2016) showed that metal-rich carbonaceous chondrites (CR, CB and CH) have a distinct signature from inner solar system objects because the former preserved a high fraction of primordial molecular cloud material, suggesting accretion in more outer regions of the solar system, similar to comets.

Moreover, similarities of reflectance spectra between Tagish Lake-like chondrites and D-type asteroids (Hiroi et al., 2001) indicate that Tagish Lake-like chondrites derived from the outermost region of the asteroid belt, which could be a likely origin for CR chondrites and 81P/Wild 2 particles. Our new data, particularly in Mg# ranges that were previously lacking (Fig. 3), further confirms the similarity between 81P/Wild 2 particles and the CR chondrite chondrule Mg#–$\Delta^{17}O$ trend. In particular, our new data point from particle T149/F2, with the highest Mg# among the five particles (99.5), displays a $\Delta^{17}O$ value of -6.9 ± 4.2‰ (2SD), indicating a reduced ^{16}O-rich end-member in 81P/Wild 2 particles that is similar to that of high Mg# chondrules in most carbonaceous chondrite groups.

If we run a Kolmogorov–Smirnov test for two variables by taking the Mg# distribution into account in addition to the $\Delta^{17}O$ distribution, the results are slightly different. When we consider only FeO-rich grains (Mg# < 90), the test shows that the distribution of 81P/Wild 2 FeO-rich grains (mean $\Delta^{17}O = -1.5 \pm 2.4$‰; 1σ) in Mg# and $\Delta^{17}O$ is the most similar to WIS91600 ($\Delta^{17}O$ =

-0.7 ± 1.5 (1σ), p-value = 0.15), is relatively close to CR chondrites ($\Delta^{17}O = 0.0 \pm 1.0$ (1σ), p-value = 0.03), and doesn't fit an OC distribution ($\Delta^{17}O = 0.4 \pm 0.3$ (1σ), p-value $\approx$ 0), nor the distribution of Acfer 094 and Yamato 81020 ($\Delta^{17}O = -2.3 \pm 0.6$ (1σ), p-value $\approx$ 0). Perhaps more concerning is that, when considering type I grains, the test shows that those from 81P/Wild 2 do not match any distributions from other chondrites. In particular, the Mg#s of 81P/Wild 2 type I grains are slightly lower (mean Mg# = 96.1 $\pm$ 1.65 (1σ)) than those from other groups (Mg# = 98.0 $\pm$ 0.93 for CR; Mg# (Yamato 81020 + Acfer 094) = 98 $\pm$ 1.9; Mg# (WIS91600) = 99.1 $\pm$ 0.33, all 1σ). In addition, CR chondrites are dominated by high Mg# silicates (type I chondrules) which represent ~99% of the total chondrule population (Weisberg et al., 1993) and ~70% of 5–30 μm olivine particles studied by Frank et al. (2014). In contrast, the 81P/Wild 2 particles with Mg# > 90 only represent a minority among silicate grains (Frank et al., 2014, estimated a fraction of 22%). This implies that, while the 81P/Wild 2 grains originated from a similar environment as that which produced chondrule silicates from CR chondrites, it was not identical. Specifically, 81P/Wild 2 grains formed in an environment generally more oxidized than that of CR chondrite chondrules, based on metal-silicate equilibria.

It is important to note that the Mg# distribution among 81P/Wild 2 particles we investigated is not fully representative of all collected samples. Indeed, particles were purposely selected in an effort to cover the widest possible range of Mg#. Such selection most likely overrepresented the amount of type I particles, which are more critical to our study, compared to type II particle abundances. However, it appears that type I particles show lower Mg#'s than CR chondrite grains, as only 2 out of 8 grains from the ^{16}O-poor cluster have a Mg# above 97, while the large majority (90%) of CR grains type I show a Mg# > 97. According to the model by Tenner et al. (2015), this indicates a dust enrichment of ≈300× for 81P/Wild 2 particles, which is slightly higher than the dust enrichment determined for CR chondrites (100–200×).

Particle T149/F7 is an amorphous grain of enstatite composition. Particles captured in aerogel underwent the peak temperature of ~2000 K for the order of ns to μs (Brownlee et al., 2006). At ~2000 K, the diffusion rate of oxygen isotope in silicate glass is of the order 10^{-4} mm^2/s (Cole and Chakraborty, 2001), which is the equivalent of 10^{-5} μm^2 per ns and too slow to diffuse more than the sub-μm. Therefore, given the rather large dimensions (5 × 7 μm) of particle T149/F7, it is safe to assume that the core of the grain preserved its pristine isotopic signature. T149/F7 shows a $\Delta^{17}O$ of 0.5 ± 2.5‰ for a Mg# of 98 (Fig. 3), while the trend suggests that for Mg# of 98, 81P/Wild2 particles should show much more negative values (≈−2‰). Those values place it slightly above the CR chondrite chondrule trend and align it more closely with the ordinary chondrite chondrule trend (Fig. 3). Its $\delta^{18}O$ and $\delta^{17}O$ (respectively 0.7 ± 1.5‰ and 0.8 ± 2.7‰) also place it on or above the TF line, in the domain of ordinary chondrites. Even though the error bars are rather large, these characteristics set it apart from the other 81P/Wild 2 particles. In addition, this particle is an amorphous grain of enstatite composition and is distinctively different to other types of particles in 81P/Wild 2, or other meteoritic analog components. It has been shown that 81P/Wild 2 collected different sources of material, and it is probable that T149/F7 came from a reservoir that was distinct from the majority of the 81P/Wild 2 particles which show more similar characteristics to CR chondrite grains.

4.2. The ^{16}O-rich enstatite particles

The pyroxene grains from track 172 show a similar ^{16}O enrichment relative to previous ^{16}O-rich particles found in 81P/Wild 2, such as the CAI Inti (track 25, McKeegan et al., 2006), a relict olivine from chondrule fragment "Gozen-sama" in track 108 (Nakamura et al., 2008), LIME olivine grains from track 57 and 77 (Nakashima et al., 2012), and a forsterite particle from track 112 (Nakamura-Messenger et al., 2011). The particles, and in particular T172/F2, contain very little CaO and Al_2O_3 (0.03–0.15% and 0.0–0.5%, respectively; Fig. 4), and are unlikely to be related to CAIs. In chondrules from primitive meteorites, relict olivine and spinel with ^{16}O-rich isotope signatures have been reported (Kunihiro et al., 2004; Wasson et al., 2004; Connolly and Huss, 2010; Ushikubo et al., 2012; Rudraswami et al., 2011; Schrader et al., 2013; Tenner et al., 2013), though significantly ^{16}O-rich enstatites have very rarely been observed. The only occurrence of ^{16}O-rich enstatite has been reported in the matrix of K chondrite Kakangari (Nagashima et al., 2015). Here we propose that ^{16}O-rich and nearly pure enstatite particles from track 172 may have a condensation origin from solar nebula gas, similar to LIME olivine and pure forsterite with ^{16}O-rich isotope signatures.

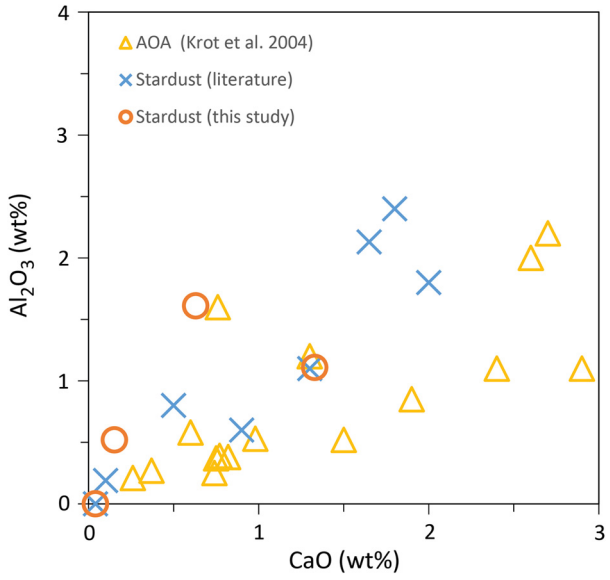

Fig. 4. Comparison between Al_2O_3 and CaO contents in AOAs and 81P/Wild 2 pyroxenes. Literature data are from Nakamura et al. (2008), Joswiak et al. (2012) and Nakashima et al. (2015) for Stardust samples, and Krot et al. (2004) for AOAs. 81P/Wild 2 particles are strongly depleted in Al_2O_3 and CaO compared to AOAs and other Stardust pyroxenes.

LIME olivines are found in IDPs, the matrices of unequilibrated chondrites (Klöck et al., 1989), and AOAs from CR chondrites (Weisberg et al., 2004) and other carbonaceous chondrites (Komatsu et al., 2015). They are considered to have formed by condensation from the solar nebula (Klöck et al., 1989; Ebel et al., 2012). For example, thermodynamic calculations predict that enstatite should condense at the same time as LIME olivine (Ebel et al., 2012). However, Ebel et al. (2012) could not constrain Mn abundances in the condensed enstatite because the partitioning of Mn in enstatite is not known. Joswiak et al. (2012) suggested several nearly pure enstatite particles, showing low contents of Al_2O_3, CaO, TiO_2, Cr_2O_3, and MnO (<1.5% in total), are candidates with possible condensate origins from the solar nebula. Elemental compositions of T172/F2 and T172/F3 match well with these pure enstatite particles (Fig. 4). Including LIME olivines, Joswiak et al. (2012) found that 27% of 81P/Wild 2 forsterite and enstatite grains (Mg# > 95) have distinct chemical characteristics with very little amounts of minor elements (less than 1.5% total oxides such as Al_2O_3, CaO, TiO_2, Cr_2O_3 and MnO). Such compositions suggest a condensation directly from the solar nebula.

Joswiak et al. (2012) previously reported a low-Ca pyroxene ($En_{99.8}$; fragment 108 of track 77) similar to that from T172/F2

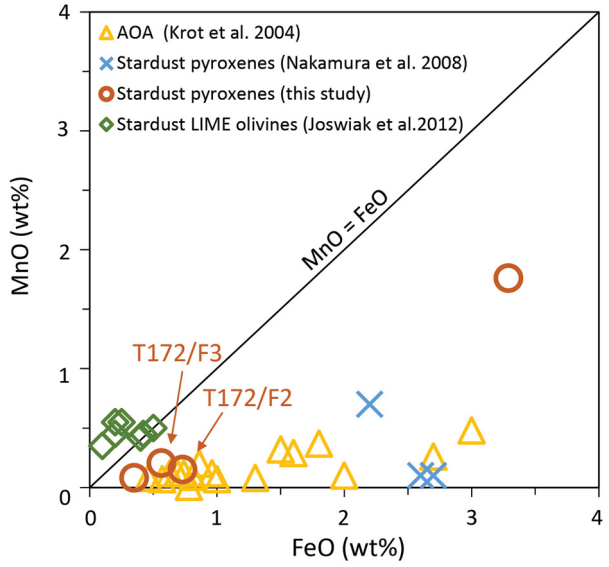

Fig. 5. FeO and MnO contents (wt%) of low-Ca pyroxenes in 81P/Wild 2 (Nakamura et al., 2008; this study) compared to those in AOAs (Krot et al., 2004). 81P/Wild 2 LIME olivine data (Joswiak et al., 2012) are shown as reference, which plot above MnO/FeO = 1 line. Both ^{16}O-rich pyroxenes (T172/F2, T172/F3) plot within a range of pyroxene in AOAs, and significantly below LIME olivines from 81P/Wild 2.

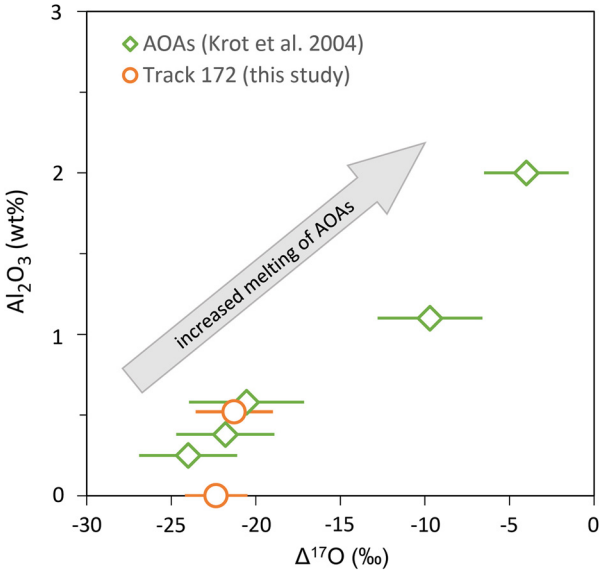

Fig. 6. Comparison between Al_2O_3 content and $\Delta^{17}O$ in AOAs (Krot et al., 2004) and 81P/Wild 2 particle T172/F2 (this study). T172/F2 appears as the end-member of the trend showing that $\Delta^{17}O$ and Al_2O_3 content increases with increased AOA degree of melting.

with low total concentrations of Al_2O_3, CaO, TiO_2, Cr_2O_3 and MnO. Although this particular pyroxene grain is too small ($\leq$1 μm) for SIMS oxygen isotope analysis, Nakashima et al. (2012) reported two LIME olivines with $\delta^{18}O \sim -50‰$ among 6 particles from the same track, suggesting possible genetic link between LIME olivine and nearly pure enstatite (T77/F108) among 81P/Wild 2 particles. However, it remains possible that the track 77 projectile might have been an aggregate of particles that formed under various environments (Nakashima et al., 2012) that are unrelated.

Recently, Messenger et al. (2015) reported a ^{16}O-rich enstatite grain (En_{99}) in a giant cluster chondritic porous IDP. It has a $\delta^{17}O = -40 \pm 9‰$, $\delta^{18}O = -44 \pm 4‰$, and has low abundances of Fe, Cr, and Mn (0.5 wt%, 0.4 wt%, and 0.1 wt%, respectively), similar to those in T172/F2 and T172/F3. Nearly pure enstatites are also observed as whiskers in IDPs, which are believed to have formed by condensation from the nebular gas (Bradley et al., 1983), but they are unfortunately are too small (sub-micron in their smaller dimension) for high precision oxygen three isotope analyses.

The rare known occurrences of ^{16}O-rich pyroxenes found in meteorites are those from amoeboid olivine aggregates (AOAs) (Krot et al., 2004), as well as the matrix of CR2 NWA 530 (Yurimoto et al., 2004), and K-grouplet chondrite Kakangari (Nagashima et al., 2015) AOAs are aggregates of forsterite olivine, FeNi metal and Ca, Al-rich minerals. They are believed to have formed in the same region as CAIs, but at relatively lower temperatures (Krot et al., 2004). Krot et al. (2004) observed the presence of low-Ca pyroxene in 10% of AOAs, mostly surrounding olivine grains, which might have formed by reactions involving olivine and surrounding SiO_2 gas. These low-Ca pyroxenes display a ^{16}O enrichment of $\Delta^{17}O < -20‰$ (Krot et al., 2005), implying that they formed from the same O-isotope reservoir as the olivine. Alternatively, pyroxene condensates could have formed directly from fractionated gas with Mg/Si ratio lower than that of solar abundance (Krot et al., 2004, 2005). However, even though it is impossible to know with confidence that isolated grains from one track were associated, the presence of LIME olivine grains in track 172 suggests this was the case.

Krot et al. (2005) showed that oxygen isotope ratios of low-Ca pyroxene in AOAs becomes ^{16}O-poor as the degree of melting in AOAs increases. They also found that ^{16}O-poor igneous low-Ca pyroxenes contain more refractory elements (CaO, Al_2O_3, and TiO_2), which are not expected to be in the gaseous phase at the condensation temperature of low-Ca pyroxene. As shown in Fig. 5, the FeO and MnO contents of T172/F2 and T172/F3 are well within the ranges observed in AOAs (Krot et al., 2004), while Al_2O_3 and CaO contents are at the lowest end compared to those in AOA low-Ca pyroxene (Fig. 4). Krot et al. (2004, 2005) show a correlation between $\Delta^{17}O$ and Al_2O_3 contents in AOA pyroxenes that increase with the degree of melting (Fig. 6). In this regard, the $\Delta^{17}O$ values and the Al_2O_3 contents of particles T172/F2 and T172/F3 are the lowest among AOA-like data, suggesting they represent the unmelted end-member of the pyroxene suite found in AOAs.

5. Conclusions

We analyzed oxygen three isotope ratios in seven silicate particles from tracks 149 and 172 of comet 81P/Wild 2. Improvement of the WiscSIMS 1280 IMS allowed for us to place the beam on small particles (5–15 μm) using ~1.5 μm spots with an aiming accuracy of 0.1 μm. Particles from track 149 show relatively ^{16}O-poor isotope compositions with $\Delta^{17}O$ values ranging from $-2‰$ to $0‰$, except for one enstatite (En_{99}) with a $\Delta^{17}O$ value of $-7‰$. These data are similar to those previously observed in 81P/Wild 2 ferromagnesian silicates, but extend the range down to $-7‰$ with the highest Mg#. These data further confirm a similar $\Delta^{17}O$ and Mg# relationship between 81P/Wild 2 particles and CR chondrite chondrules, including the existence of a high Mg# (>98) and low $\Delta^{17}O$ ($\leq -5‰$) component that is commonly observed among chondrules from carbonaceous chondrites. However, FeO-poor (Mg# < 90) particles are less abundant in 81P/Wild 2 silicates than in CR chondrites, implying that environments of formation for the 81P/Wild 2 particles were more oxidized.

The two particles from track 172 are the first ^{16}O-rich pyroxenes found among 81P/Wild 2 samples, with a $\Delta^{17}O$ of ~$-22‰$, or as low as other ^{16}O-rich 81P/Wild 2 particles including LIME olivine. Their oxygen isotopic ratios and elemental compositions are in good agreement with those of pyroxene grains found in AOAs, indicating a link between ^{16}O-rich ferromagnesian silicate particles in 81P/Wild 2 and those in AOAs.

Acknowledgements

The authors thank CAPTEM for the allocation of 81P/Wild 2 particles, Richard K. Noll for assistance for FIB and FE-SEM observations, Jim. Kern for SIMS support and profilometer assistance, as well as Peter E. Sobol and Neal E. Lord for the hardware and software development of the NanoDeflector. The authors gratefully acknowledge use of facilities and instrumentation supported by NSF through the University of Wisconsin Materials Research Science and Engineering Center (DMR-1121288). This work is supported by NASA programs (NK: NNX13AD15G, DB: NNX14AF28G). WiscSIMS is partly supported by NSF (EAR03-19230, EAR13-55590).

Appendix A. Supplementary material

Supplementary material related to this article can be found online at http://dx.doi.org/10.1016/j.epsl.2017.02.045.

References

Bradley, J.P., Brownlee, D.E., Veblen, D.R., 1983. Pyroxene whiskers and platelets in interplanetary dust: evidence of vapour phase growth. Nature 301, 473–477. http://dx.doi.org/10.1038/301473a0.

Bridges, J.C., Changela, H.G., Nayakshin, S., Starkey, N.A., Franchi, I.A., 2012. Chondrule fragments from Comet Wild2: evidence for high temperature processing in the outer Solar System. Earth Planet. Sci. Lett. 341–344, 186–194. http://dx.doi.org/10.1016/j.epsl.2012.06.011.

Brownlee, D., Tsou, P., Aléon, J., Alexander, C.M.O., Araki, T., Bajt, S., Baratta, G.A., Bastien, R., Bland, P., Bleuet, P., Borg, J., Bradley, J.P., Brearley, A., Brenker, F., Brennan, S., Bridges, J.C., Browning, N.D., Brucato, J.R., Bullock, E., Burchell, M.J., Busemann, H., Butterworth, A., Chaussidon, M., Cheuvront, A., Chi, M., Cintala, M.J., Clark, B.C., Clemett, S.J., Cody, G., Colangeli, L., Cooper, G., Cordier, P., Daghlian, C., Dai, Z., D'Hendecourt, L., Djouadi, Z., Dominguez, G., Duxbury, T., Dworkin, J.P., Ebel, D.S., Economou, T.E., Fakra, S., Fairey, S.A.J., Fallon, S., Ferrini, G., Ferroir, T., Fleckenstein, H., Floss, C., Flynn, G., Franchi, I.A., Fries, M., Gainsforth, Z., Gallien, J.-P., Genge, M., Gilles, M.K., Gillet, P., Gilmour, J., Glavin, D.P., Gounelle, M., Grady, M.M., Graham, G.A., Grant, P.G., Green, S.F., Grossemy, F., Grossman, L., Grossman, J.N., Guan, Y., Hagiya, K., Harvey, R., Heck, P., Herzog, G.F., Hoppe, P., Hörz, F., Huth, J., Hutcheon, I.D., Ignatyev, K., Ishii, H., Ito, M., Jacob, D., Jacobsen, C., Jacobsen, S., Jones, S., Joswiak, D., Jurewicz, A., Kearsley, A.T., Keller, L.P., Khodja, H., Kilcoyne, A.L.D., Kissel, J., Krot, A., Langenhorst, F., Lanzirotti, A., Le, L., Leshin, L.A., Leitner, J., Lemelle, L., Leroux, H., Liu, M.-C., Luening, K., Lyon, I., MacPherson, G., Marcus, M.A., Marhas, K., Marty, B., Matrajt, G., McKeegan, K., Meibom, A., Mennella, V., Messenger, K., Messenger, S., Mikouchi, T., Mostefaoui, S., Nakamura, T., Nakano, T., Newville, M., Nittler, L.R., Ohnishi, I., Ohsumi, K., Okudaira, K., Papanastassiou, D.A., Palma, R., Palumbo, M.E., Pepin, R.O., Perkins, D., Perronnet, M., Pianetta, P., Rao, W., Rietmeijer, F.J.M., Robert, F., Rost, D., Rotundi, A., Ryan, R., Sandford, S.A., Schwandt, C.S., See, T.H., Schlutter, D., Sheffield-Parker, J., Simionovici, A., Simon, S., Sitnitsky, I., Snead, C.J., Spencer, M.K., Stadermann, F.J., Steele, A., Stephan, T., Stroud, R., Susini, J., Sutton, S.R., Suzuki, Y., Taheri, M., Taylor, S., Teslich, N., Tomeoka, K., Tomioka, N., Toppani, A., Trigo-Rodríguez, J.M., Troadec, D., Tsuchiyama, A., Tuzzolino, A.J., Tyliszczak, T., Uesugi, K., Velbel, M., Vellenga, J., Vicenzi, E., Vincze, L., Warren, J., Weber, I., Weisberg, M., Westphal, A.J., Wirick, S., Wooden, D., Wopenka, B., Wozniakiewicz, P., Wright, I., Yabuta, H., Yano, H., Young, E.D., Zare, R.N., Zega, T., Ziegler, K., Zimmerman, L., Zinner, E., Zolensky, M., 2006. Comet 81P/Wild 2 under a microscope. Science 314, 1711–1716. http://dx.doi.org/10.1126/science.1135840.

Burchell, M.J., Fairey, S.A.J., Wozniakiewicz, P., Brownlee, D.E., Hörz, F., Kearsley, A.T., See, T.H., Tsou, P., Westphal, A., Green, S.F., Trigo-Rodríguez, J.M., Domingúez, G., 2008. Characteristics of cometary dust tracks in Stardust aerogel and laboratory calibrations. Meteorit. Planet. Sci. 43, 23–40. http://dx.doi.org/10.1111/j.1945-5100.2008.tb00608.x.

Ciesla, F.J., 2007. Outward transport of high-temperature materials around the Midplane of the Solar Nebula. Science 318, 613–615. http://dx.doi.org/10.1126/science.1147273.

Clayton, R.N., Onuma, N., Grossman, L., Mayeda, T.K., 1977. Distribution of the presolar component in Allende and other carbonaceous chondrites. Earth Planet. Sci. Lett. 34, 209–224. http://dx.doi.org/10.1016/0012-821X(77)90005-X.

Cole, D.R., Chakraborty, S., 2001. Rates and mechanisms of isotopic exchange. Rev. Mineral. Geochem. 43, 83–223. http://dx.doi.org/10.2138/gsrmg.43.1.83.

Connolly Jr., H.C., Huss, G.R., 2010. Compositional evolution of the protoplanetary disk: oxygen isotopes of type-II chondrules from CR2 chondrites. Geochim. Cosmochim. Acta 74, 2473–2483. http://dx.doi.org/10.1016/j.gca.2010.01.005.

Ebel, D.S., Weisberg, M.K., Beckett, J.R., 2012. Thermochemical stability of low-iron, manganese-enriched olivine in astrophysical environments. Meteorit. Planet. Sci. 47, 585–593. http://dx.doi.org/10.1111/j.1945-5100.2012.01347.x.

Frank, D.R., Zolensky, M.E., Le, L., 2014. Olivine in terminal particles of Stardust aerogel tracks and analogous grains in chondrite matrix. Geochim. Cosmochim. Acta 142, 240–259. http://dx.doi.org/10.1016/j.gca.2014.05.037.

Gainsforth, Z., Butterworth, A.L., Stodolna, J., Westphal, A.J., Huss, G.R., Nagashima, K., Ogliore, R., Brownlee, D.E., Joswiak, D., Tyliszczak, T., Simionovici, A.S., 2015. Constraints on the formation environment of two chondrule-like igneous particles from comet 81P/Wild 2. Meteorit. Planet. Sci. 50, 976–1004. http://dx.doi.org/10.1111/maps.12445.

Greenberg, J.M., Li, A., 1999. Morphological structure and chemical composition of cometary nuclei and dust. Space Sci. Rev. 90, 149–161. http://dx.doi.org/10.1023/A:1005298014670.

Hiroi, T., Zolensky, M.E., Pieters, C.M., 2001. The Tagish Lake Meteorite: a possible sample from a D-type asteroid. Science 293, 2234–2236. http://dx.doi.org/10.1126/science.1063734.

Joswiak, D.J., Brownlee, D.E., Matrajt, G., Westphal, A.J., Snead, C.J., Gainsforth, Z., 2012. Comprehensive examination of large mineral and rock fragments in Stardust tracks: mineralogy, analogous extraterrestrial materials, and source regions. Meteorit. Planet. Sci. 47, 471–524. http://dx.doi.org/10.1111/j.1945-5100.2012.01337.x.

Joswiak, D.J., Nakashima, D., Brownlee, D.E., Matrajt, G., Ushikubo, T., Kita, N.T., Messenger, S., Ito, M., 2014. Terminal particle from Stardust track 130: probable Al-rich chondrule fragment from comet Wild 2. Geochim. Cosmochim. Acta 144, 277–298. http://dx.doi.org/10.1016/j.gca.2014.08.017.

Kita, N.T., Nagahara, H., Tachibana, S., Tomomura, S., Spicuzza, M.J., Fournelle, J.H., Valley, J.W., 2010. High precision SIMS oxygen three isotope study of chondrules in LL3 chondrites: role of ambient gas during chondrule formation. Geochim. Cosmochim. Acta 74, 6610–6635. http://dx.doi.org/10.1016/j.gca.2010.08.011.

Kita, N.T., Ushikubo, T., Fu, B., Valley, J.W., 2009. High precision SIMS oxygen isotope analysis and the effect of sample topography. Chem. Geol. 264, 43–57. http://dx.doi.org/10.1016/j.chemgeo.2009.02.012.

Klöck, W., Thomas, K.L., McKay, D.S., Palme, H., 1989. Unusual olivine and pyroxene composition in interplanetary dust and unequilibrated ordinary chondrites. Nature 339, 126–128. http://dx.doi.org/10.1038/339126a0.

Komatsu, M., Fagan, T.J., Mikouchi, T., Petaev, M.I., Zolensky, M.E., 2015. LIME silicates in amoeboid olivine aggregates in carbonaceous chondrites: indicator of nebular and asteroidal processes. Meteorit. Planet. Sci. 50, 1271–1294. http://dx.doi.org/10.1111/maps.12460.

Krot, A.N., Fagan, T.J., Nagashima, K., Petaev, M.I., Yurimoto, H., 2005. Origin of low-Ca pyroxene in amoeboid olivine aggregates: evidence from oxygen isotopic compositions. Geochim. Cosmochim. Acta 69, 1873–1881. http://dx.doi.org/10.1016/j.gca.2004.06.046.

Krot, A.N., Petaev, M.I., Yurimoto, H., 2004. Amoeboid olivine aggregates with low-Ca pyroxenes: a genetic link between refractory inclusions and chondrules? Geochim. Cosmochim. Acta 68, 1923–1941. http://dx.doi.org/10.1016/j.gca.2003.10.026.

Kunihiro, T., Rubin, A.E., McKeegan, K.D., Wasson, J.T., 2004. Oxygen-isotopic compositions of relict and host grains in chondrules in the Yamato 81020 CO3.0 chondrite. Geochim. Cosmochim. Acta 68, 3599–3606. http://dx.doi.org/10.1016/j.gca.2004.02.011.

Leitner, J., Hoppe, P., Heck, P.R., 2010. First discovery of presolar material of possible supernova origin in impact residues from Comet 81P/Wild 2. In: Lunar and Planetary Science Conference, p. 1607.

Matrajt, G., Ito, M., Wirick, S., Messenger, S., Brownlee, D.E., Joswiak, D., Flynn, G., Sandford, S., Snead, C., Westphal, A., 2008. Carbon investigation of two Stardust particles: a TEM, NanoSIMS, and XANES study. Meteorit. Planet. Sci. 43, 315–334. http://dx.doi.org/10.1111/j.1945-5100.2008.tb00625.x.

McKeegan, K.D., Aléon, J., Bradley, J., Brownlee, D., Busemann, H., Butterworth, A., Chaussidon, M., Fallon, S., Floss, C., Gilmour, J., Gounelle, M., Graham, G., Guan, Y., Heck, P.R., Hoppe, P., Hutcheon, I.D., Huth, J., Ishii, H., Ito, M., Jacobsen, S.B., Kearsley, A., Leshin, L.A., Liu, M.-C., Lyon, I., Marhas, K., Marty, B., Matrajt, G., Meibom, A., Messenger, S., Mostefaoui, S., Mukhopadhyay, S., Nakamura-Messenger, K., Nittler, L., Palma, R., Pepin, R.O., Papanastassiou, D.A., Robert, F., Schlutter, D., Snead, C.J., Stadermann, F.J., Stroud, R., Tsou, P., Westphal, A., Young, E.D., Ziegler, K., Zimmermann, L., Zinner, E., 2006. Isotopic compositions of cometary matter returned by stardust. Science 314, 1724–1728. http://dx.doi.org/10.1126/science.1135992.

Messenger, S. Brownlee, D.E. Joswiak, D.J. Nguyen, A.N., 2015. Nebular and interstellar materials in a Giant Cluster IDP of probable cometary origin. LPI Contrib. 1856, 5365.

Messenger, S., Joswiak, D., Ito, M., Matrajt, G., Brownlee, D.E., 2009. Discovery of presolar SiC from Comet WILD-2. In: Lunar and Planetary Science Conference, p. 1790.

Nagashima, K., Krot, A.N., Huss, G.R., 2015. Oxygen-isotope compositions of chondrule phenocrysts and matrix grains in Kakangari K-grouplet chondrite: implication to a chondrule-matrix genetic relationship. Geochim. Cosmochim. Acta 151, 49–67. http://dx.doi.org/10.1016/j.gca.2014.12.012.

Nakamura, T., Noguchi, T., Tsuchiyama, A., Ushikubo, T., Kita, N.T., Valley, J.W., Zolensky, M.E., Kakazu, Y., Sakamoto, K., Mashio, E., Uesugi, K., Nakano, T., 2008. Chondrulelike objects in short-period Comet 81P/Wild 2. Science 321, 1664–1667. http://dx.doi.org/10.1126/science.1160995.

Nakamura-Messenger, K., Keller, L.P., Clemett, S.J., Messenger, S., Ito, M., 2011. Nanometer-scale anatomy of entire Stardust tracks. Meteorit. Planet. Sci. 46, 1033–1051. http://dx.doi.org/10.1111/j.1945-5100.2011.01211.x.

Nakashima, D., Ushikubo, T., Zolensky, M.E., Weisberg, M.K., Joswiak, D.J., Brownlee, D.E., Matrajt, G., Kita, N.T., 2011. High precision oxygen three isotope analysis of Wild-2 particles and anhydrous chondritic interplanetary dust particles.

Nakashima, D., Ushikubo, T., Joswiak, D.J., Brownlee, D.E., Matrajt, G., Weisberg, M.K., Zolensky, M.E., Kita, N.T., 2012. Oxygen isotopes in crystalline silicates of comet Wild 2: a comparison of oxygen isotope systematics between Wild 2 particles and chondritic materials. Earth Planet. Sci. Lett. 357–358, 355–365. http://dx.doi.org/10.1016/j.epsl.2012.09.041.

Nakashima, D., Ushikubo, T., Kita, N.T., Weisberg, M.K., Zolensky, M.E., Ebel, D.S., 2015. Late formation of a comet Wild 2 crystalline silicate particle, Pyxie, inferred from Al–Mg chronology of plagioclase. Earth Planet. Sci. Lett. 410, 54–61. http://dx.doi.org/10.1016/j.epsl.2014.11.020.

Ogliore, R.C., Huss, G.R., Nagashima, K., Butterworth, A.L., Gainsforth, Z., Stodolna, J., Westphal, A.J., Joswiak, D., Tyliszczak, T., 2012. Incorporation of a late-forming chondrule into Comet Wild 2. Astrophys. J. Lett. 745, L19. http://dx.doi.org/10.1088/2041-8205/745/2/L19.

Ogliore, R.C., Nagashima, K., Huss, G.R., Westphal, A.J., Gainsforth, Z., Butterworth, A.L., 2015. Oxygen isotopic composition of coarse- and fine-grained material from Comet 81P/Wild 2. Geochim. Cosmochim. Acta 166, 74–91.

Rudraswami, N.G., Ushikubo, T., Nakashima, D., Kita, N.T., 2011. Oxygen isotope systematics of chondrules in the Allende CV3 chondrite: high precision ion microprobe studies. Geochim. Cosmochim. Acta 75, 7596–7611. http://dx.doi.org/10.1016/j.gca.2011.09.035.

Sandford, S.A., Aléon, J., Alexander, C.M.O., Araki, T., Bajt, S., Baratta, G.A., Borg, J., Bradley, J.P., Brownlee, D.E., Brucato, J.R., Burchell, M.J., Busemann, H., Butterworth, A., Clemett, S.J., Cody, G., Colangeli, L., Cooper, G., D'Hendecourt, L., Djouadi, Z., Dworkin, J.P., Ferrini, G., Fleckenstein, H., Flynn, G.J., Franchi, I.A., Fries, M., Gilles, M.K., Glavin, D.P., Gounelle, M., Grossemy, F., Jacobsen, C., Keller, L.P., Kilcoyne, A.L.D., Leitner, J., Matrajt, G., Meibom, A., Mennella, V., Mostefaoui, S., Nittler, L.R., Palumbo, M.E., Papanastassiou, D.A., Robert, F., Rotundi, A., Snead, C.J., Spencer, M.K., Stadermann, F.J., Steele, A., Stephan, T., Tsou, P., Tyliszczak, T., Westphal, A.J., Wirick, S., Wopenka, B., Yabuta, H., Zare, R.N., Zolensky, M.E., 2006. Organics captured from Comet 81P/Wild 2 by the Stardust spacecraft. Science 314, 1720–1724. http://dx.doi.org/10.1126/science.1135841.

Schrader, D.L., Connolly Jr., H.C., Lauretta, D.S., Nagashima, K., Huss, G.R., Davidson, J., Domanik, K.J., 2013. The formation and alteration of the Renazzo-like carbonaceous chondrites II: linking O-isotope composition and oxidation state of chondrule olivine. Geochim. Cosmochim. Acta 101, 302–327. http://dx.doi.org/10.1016/j.gca.2012.09.045.

Tenner, T.J., Nakashima, D., Ushikubo, T., Kita, N.T., Weisberg, M.K., 2015. Oxygen isotope ratios of FeO-poor chondrules in CR3 chondrites: influence of dust enrichment and H_2O during chondrule formation. Geochim. Cosmochim. Acta 148, 228–250. http://dx.doi.org/10.1016/j.gca.2014.09.025.

Tenner, T.J., Ushikubo, T., Kurahashi, E., Kita, N.T., Nagahara, H., 2013. Oxygen isotope systematics of chondrule phenocrysts from the CO3.0 chondrite Yamato 81020: evidence for two distinct oxygen isotope reservoirs. Geochim. Cosmochim. Acta 102, 226–245. http://dx.doi.org/10.1016/j.gca.2012.10.034.

Ushikubo, T., Kimura, M., Kita, N.T., Valley, J.W., 2012. Primordial oxygen isotope reservoirs of the solar nebula recorded in chondrules in Acfer 094 carbonaceous chondrite. Geochim. Cosmochim. Acta 90, 242–264. http://dx.doi.org/10.1016/j.gca.2012.05.010.

Van Kooten, E.M.M.E., Wielandt, D., Schiller, M., Nagashima, K., Thomen, A., Larsen, K.K., Olsen, M.B., Nordlund, Å., Krot, A.N., Bizzarro, M., 2016. Isotopic evidence for primordial molecular cloud material in metal-rich carbonaceous chondrites. Proc. Natl. Acad. Sci. 113, 2011–2016. http://dx.doi.org/10.1073/pnas.1518183113.

Wasson, J.T., Rubin, A.E., Yurimoto, H., 2004. Evidence in CO3.0 chondrules for a drift in the O isotopic composition of the solar nebula. Meteorit. Planet. Sci. 39, 1591–1598. http://dx.doi.org/10.1111/j.1945-5100.2004.tb00129.x.

Weisberg, M.K., Connolly, H.C., Ebel, D.S., 2004. Petrology and origin of amoeboid olivine aggregates in CR chondrites. Meteorit. Planet. Sci. 39, 1741–1753. http://dx.doi.org/10.1111/j.1945-5100.2004.tb00070.x.

Weisberg, M.K., Ebel, D.S., Connolly Jr., H.C., Kita, N.T., Ushikubo, T., 2011. Petrology and oxygen isotope compositions of chondrules in E3 chondrites. Geochim. Cosmochim. Acta 75, 6556–6569. http://dx.doi.org/10.1016/j.gca.2011.08.040.

Weisberg, M.K., Prinz, M., Clayton, R.N., Mayeda, T.K., 1993. The CR (Renazzo-type) carbonaceous chondrite group and its implications. Geochim. Cosmochim. Acta 57, 1567–1586. http://dx.doi.org/10.1016/0016-7037(93)90013-M.

Yamanobe, M., Nakamura, T., Nakashima, D., 2016. Oxygen Isotope ratios of chondrules and isolated forsterite and olivine grains in the WIS91600 carbonaceous chondrite from D-type asteroid. In: 47th Lunar and Planetary Science Conference. Abstract #1861.

Yang, L., Ciesla, F.J., 2012. The effects of disk building on the distributions of refractory materials in the solar nebula. Meteorit. Planet. Sci. 47, 99–119. http://dx.doi.org/10.1111/j.1945-5100.2011.01315.x.

Young, E.D., Russell, S.S., 1998. Oxygen reservoirs in the Early Solar Nebula inferred from an Allende CAI. Science 282, 452–455. http://dx.doi.org/10.1126/science.282.5388.452.

Yurimoto, H., Nagashima, K., Emori, H., 2004. Radial migration of materials from inner to outer solar nebula: evidence from meteorite matrix. Lunar Planet. Sci. 35. Abstract #1649.

Zolensky, M.E., Zega, T.J., Yano, H., Wirick, S., Westphal, A.J., Weisberg, M.K., Weber, I., Warren, J.L., Velbel, M.A., Tsuchiyama, A., Tsou, P., Toppani, A., Tomioka, N., Tomeoka, K., Teslich, N., Taheri, M., Susini, J., Stroud, R., Stephan, T., Stadermann, F.J., Snead, C.J., Simon, S.B., Simionovici, A., See, T.H., Robert, F., Rietmeijer, F.J.M., Rao, W., Perronnet, M.C., Papanastassiou, D.A., Okudaira, K., Ohsumi, K., Ohnishi, I., Nakamura-Messenger, K., Nakamura, T., Mostefaoui, S., Mikouchi, T., Meibom, A., Matrajt, G., Marcus, M.A., Leroux, H., Lemelle, L., Le, L., Lanzirotti, A., Langenhorst, F., Krot, A.N., Keller, L.P., Kearsley, A.T., Joswiak, D., Jacob, D., Ishii, H., Harvey, R., Hagiya, K., Grossman, L., Grossman, J.N., Graham, G.A., Gounelle, M., Gillet, P., Genge, M.J., Flynn, G., Ferroir, T., Fallon, S., Ebel, D.S., Dai, Z.R., Cordier, P., Clark, B., Chi, M., Butterworth, A.L., Brownlee, D.E., Bridges, J.C., Brennan, S., Brearley, A., Bradley, J.P., Bleuet, P., Bland, P.A., Bastien, R., 2006. Mineralogy and petrology of Comet 81P/Wild 2 nucleus samples. Science 314, 1735–1739. http://dx.doi.org/10.1126/science.1135842.